

Morphological response to climate-induced flood-event variability in a subarctic river

3

4 **Linnea Blåfield**¹, Carlos Gonzales-Inca¹, Petteri Alho^{1,2}, Elina Kasvi¹

5

6 ¹Department of Geography and Geology, University of Turku, Finland

7 ²Finnish Geospatial Research Institute FGI, National Land Survey of Finland, Espoo,
8 Finland

9 Correspondence to: Linnea Blåfield, linnea.m.blafield@utu.fi

10

11 Keywords: Sediment transport hysteresis, Computational modelling, Flood sequencing,
12 Hydroclimatics

13

14 Highlights:

- 15 - Sediment transport hysteresis pattern is dependent on the number and volume of flood
16 peak sequences
- 17 - Flood-event type significantly impacts the rivers morphological response
- 18 - Increase of multi-peaking flood-events, mean temperature, and changing precipitation
19 patterns affects the future river system stability
- 20 - Hydrograph shape can be associated to specific preceding climatic conditions

21

22 Abstract

23 This study examined the effects of climate-induced flood-event variability and peak
24 sequencing on morphological response and sediment transport hysteresis patterns in a
25 subarctic river. We classified 32 years of discharge hydrographs from a subarctic river
26 according to their spring flood hydrograph shapes and peak sequences. These classified
27 flood-event types and their frequencies were statistically analysed against seasonal and
28 annual climatic conditions from the corresponding time periods. Morphodynamic modelling
29 was employed to examine the effects of flood-event hydrograph shape and sequencing on
30 morphological response and sediment transport hysteresis patterns during floods. The
31 findings highlight the critical role that hydrograph shape and sequencing play in influencing
32 river morphology and sediment transport dynamics, as each flood-event type produced
33 distinct sediment transport hysteresis patterns and morphological outcomes. Double-
34 peaking floods resulted in relatively more heterogeneous and complex morphological
35 outcome compared to single-peaking floods. Variance and trend analyses revealed that
36 prevailing climatic conditions significantly influence the hydrograph shapes of spring flood

events. Annual mean temperature, total precipitation, and snow accumulation, together with cold season mean temperature, spring rainfall, and May cumulative temperature, had the greatest impact on the type of spring flood event observed. Significant increasing trends were identified in annual and spring mean temperatures, spring rainfall, and the frequency of rain-on-snow events. This suggests that ongoing climatic shifts are actively modifying the nature of spring flood events, favouring more complex and variable hydrograph forms. Consequently, future sediment transport and morphological evolution in subarctic rivers are likely to become increasingly event-driven, less predictable, and more sensitive to interannual climatic variability. These changes emphasise the need for adaptive management strategies that can accommodate the emerging hydrological and geomorphological dynamics under a changing climate.

1. Introduction

Hydrological variability significantly affects riverine sediment fluxes, especially in cold climate rivers where sediment transport is highly seasonal, occurring predominantly during spring floods (Syvitski, 2002; Favaro & Lamoureux, 2015; Zhang et al., 2022). Snowmelt-driven spring floods carry majority of the annual sediment budget and therefore, they define the timing and volume of sediment transport and ultimately the whole river morphology. Currently, cold climate rivers are experiencing rapid shifts in hydroclimatic conditions, influencing the flow-sediment interaction in the river systems (Meriö et al., 2019; Beel et al., 2021; Li et al., 2021; Zhang et al., 2023; Blåfield et al., 2024a). As hydroclimatic conditions evolve, the characteristics of flood-events are also changing with implications to the traditional sediment transport dynamics. For instance, the shift in the snow-to-precipitation ratio and changes in the timing and intensity of snowmelt have already altered flood hydrographs i.e., the shape, magnitude, duration, and sediment transport capacity of events in cold-climate rivers (Wohl et al., 2017; Gohari et al., 2021; Hopwood et al., 2021; Zhang et al., 2022; Blåfield et al., 2024a; Lintunen et al., 2024). Flood-events are usually classified by their generating processes (e.g., intense precipitation, snowmelt, rain-on-snow, ice jamming, dam break etc.), with less emphasis on the event type and sequences itself. Previous studies (Viglione et al., 2010; Fischer et al., 2019; Gohari et al., 2022), however, have reported that ongoing regime shifts have altered flood-event shapes. Over the past century, multi-peaking floods have become more common, not only in central Europe, but also in high-latitude regions.

In multi-peaking floods, the order and duration of different peaks significantly affects the sediment transport volume and the pattern of sediment transport hysteresis because the flow conditions control when, how much, and what type of sediment is mobilised, reworked, or deposited within the river system (Mao, 2018). Therefore, understanding the contribution of flood-event sequences to sediment transport is crucial for predicting the impact of climate change on fluvial sediment dynamics and the morphological response of river systems (Mao, 2012; Karimaei Tabarestani & Zarrati, 2015). This is particularly important in cold-climate rivers, which have historically experienced a single major snowmelt-driven flood and low sediment loads. However, due to hydroclimatic regime shifts, altered fluvial dynamics and possible permafrost or glacier melt, these regions are increasingly becoming hotspots for

elevated sediment transport (Syvitski et al., 2002; Li et al. 2021; Zhang et al., 2022). Recent studies indicate that migration rates of large, sinuous rivers in the Arctic permafrost region have slowed by 20% during the past 50 years due to decreased fluvial energy and increased bank shrubification (Ielpi et al., 2023). Contrasting findings have been made on the Tibetan Plateau where migration rates have increased by 34% due to increased discharge volumes and river bank destabilisation caused by permafrost melt (Sha et al., 2025). In boreal-subarctic regions, where the focus of this study is, the fluvial activity and extreme discharge events outside the spring flood season have increased while spring flood peaks have decreased significantly (Korhonen & Kuusisto, 2010; Lintunen et al., 2024). The increased fluvial activity outside traditional flood season is caused by increasing number of extreme rainfall events (Nikulin et al., 2011) which are intensifying bank erosion and sediment transport (Kärkkäinen & Lotsari, 2022). However, the annual total volume of water has not yet changed (Lintunen et al., 2024). All these findings suggest that climate change has diverse impacts on fluvial dynamics across the high-latitude region, and therefore more focus should be paid sediment transport dynamics and the hysteresis pattern under evolving discharge conditions. Understanding these processes is essential because sediment transport not only shapes river morphology but also governs aquatic habitats, influences nutrient fluxes, and affects infrastructure stability.

One effective way to evaluate the sediment transport process and morphological response of the river channel is through analysis of sediment transport hysteresis patterns, which reflect the sediment transport affected by riverbed structure, sediment composition and availability at different stages of the flow hydrograph (Williams, 1989; Reesink & Bridge, 2011; Gunsolus & Binns, 2017). In cold climate rivers various types of sediment transport hysteresis have been observed due to highly seasonal and varying sediment availability between catchments (Vatne et al., 2008; Kociuba, 2021; Wenng et al., 2021; Zhang et al., 2021; Liébault et al., 2022). Yet, measuring bedload and hysteresis in natural rivers during high flows remains challenging and is prone to biases. As a result, long time series of bedload transport and hysteresis are scarce worldwide (Mao, 2018; Zhang et al., 2023). Thus, we rely on laboratory experiments, computational modelling, and field measurements of suspended load when evaluating and measuring the current, and predicting the future sediment fluxes and morphodynamic response of the river channels.

The ability to evaluate and predict the effects of climate change on sediment transport rates and morphological response is essential not only for understanding fluvial morphodynamics, such as channel stability and sediment connectivity but also for a wide range of river engineering and management applications (Mao, 2018; Gupta et al., 2022; Najafi et al., 2021). Therefore, this study aims to: i) Analyse and classify the variation in flood-event hydrographs over the past 32-years in a subarctic river, ii) Link the flood-events to seasonal and annual climate conditions, and iii) Evaluate the channels morphological response distinctive to each flood-event type utilising morphodynamic modelling and sediment transport hysteresis analysis. We expect to detect linkages between the flood-event hydrograph shape and climatic conditions as well as diverse patterns of morphological response and sediment transport hysteresis. The study was conducted on a river reach in

125 Finland, located at 70° North latitude. Despite its high latitude, Finland has a relatively mild
126 climate compared to other regions at similar latitudes, such as Siberia, northern Canada,
127 and Alaska, largely due to the warming influence of the Gulf Stream and the North Atlantic
128 Drift. As a result, Finland is mostly free of permafrost (Luoto et al., 2004), although small
129 areas of permafrost exist in the form of palsas mires. These palsas are primarily found in
130 north-western Finland (Seppälä, 1997; Gislås et al., 2017; Verdonen et al., 2023).
131 Nevertheless, Finland experiences seasonally frozen ground for periods ranging from four
132 (South) to eight (North) months each year (Rimali, 2019).

133

134 **2. Study area**

135 The meandering and unregulated Pulmanki River locates in northern Finland (Fig. 1A)The
136 river is a tributary to Tana River which flows into the Arctic Ocean on Norwegian side of the
137 border (Fig. 1A). The river is divided into two separate sections by the Lake Pulmankijärvi
138 (Fig. 1B). The area of interest in this study is a 6-kilometre-long reach on the upper course
139 of the Pulmanki River approximately 13 meters above the mean sea level (a.m.s.l) (Fig. 1B).
140 This reach consists of 13 meander bends with a reach sinuosity of 2.4. The bankfull width
141 of the river varies between 60 to 100 metres, depending on the valley confinement. The river
142 flows through glaciolacustrine and glacio-fluvial sediments deposited on the fjord bottom
143 after the final wasting of Fennoscandian ice sheet (Mansikkaniemi, 1967; Hirvas et al., 1988;
144 Johansson et al., 2007). The D50 value of the channel bed material ranges from 0.1 mm to
145 4 mm and a sandy bedload (D50 0.43 mm) dominates the sediment transport. The amount
146 of suspended material is minimal (0-180 mg/L), even during the spring flood (Lotsari et al.,
147 2020). The bed morphology is typical for sand bed rivers and consists of dunes, ripples,
148 pools, and riffles, the bed is unvegetated and mobile through the year. The channel is frozen
149 from October to May, and the seasonal discharge ranges from 0.5 to 100 m³/s. A spring
150 flood generated by the snowmelt occurs annually in late-May or early June. Lower discharge
151 peaks are associated with precipitation events during July, August and September. The river
152 belongs to subarctic-nival hydrological regime (Linsinger and Wohl, 2009) and to Köppen
153 climate class: "Cold, without dry season, but with cold summer" as the area is affected by
154 the great Asian continent and both the Atlantic Ocean and the Gulf Stream. Based on the
155 Nordic permafrost model by Gislås et al., (2017) majority of the catchment is permafrost
156 free (Fig. 1C). The south-western corner has 10-50 % probability of sporadic permafrost
157 according to the model results based on land cover, snow accumulation and temperature
158 data. However, no confirmed field observations of sporadic permafrost from the area exist,
159 and therefore we consider this catchment and river system as non-permafrost river.

160

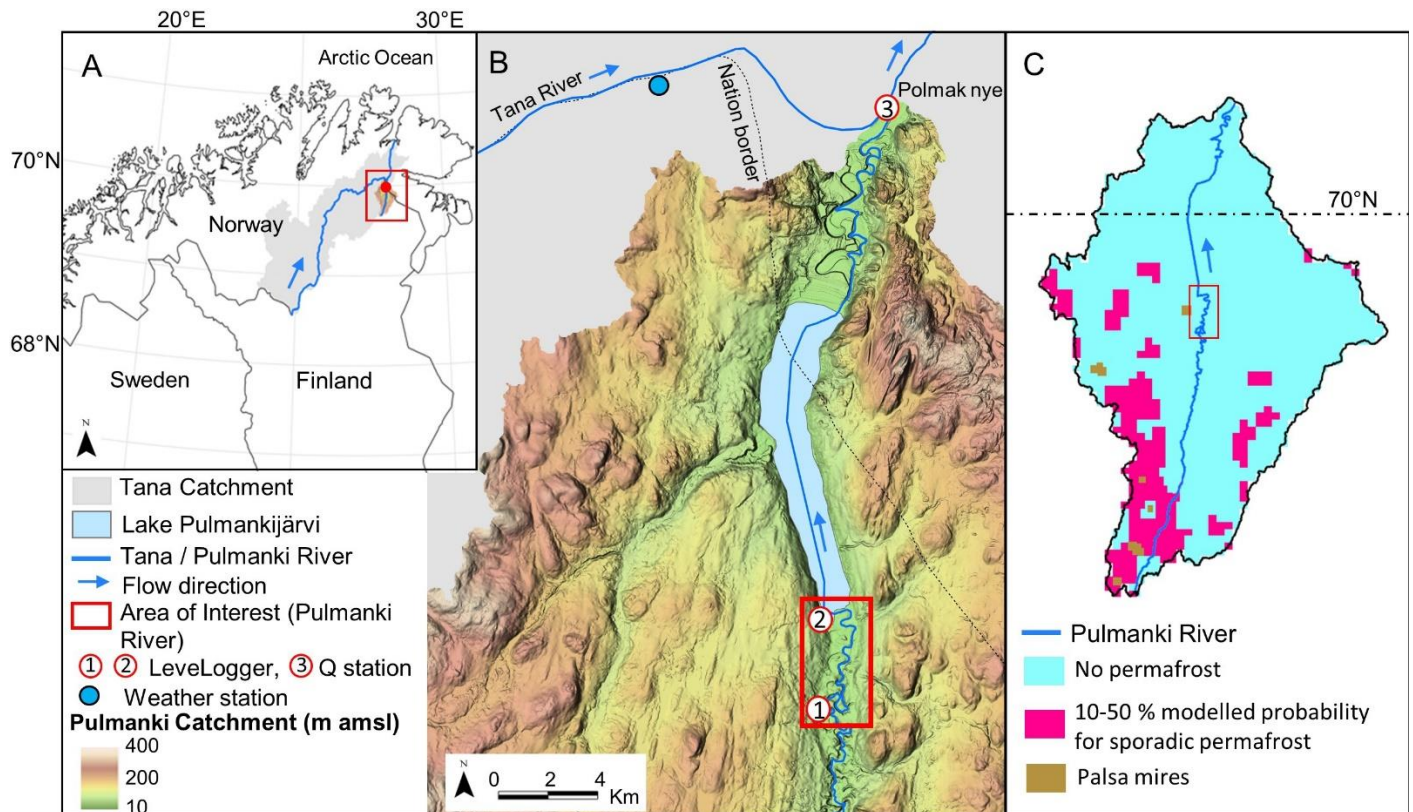


Figure 1. Area of interest. A) The study area's location in the Northern most Finland. B) Model area is marked with rectangle, and the locations of LeveLogger sensors (LL), discharge (Q), and weather station with circular markers. C) The probability of sporadic permafrost within the catchment based on the Nordic permafrost model by Gissnäs et al., 2017. Pulmanki catchment 2x2 m DEM by National Land Survey of Finland.

3. Data & Methods

Discharge hydrographs of the years 1992-2023 were analysed and classified to recognise variability in spring flood-event shapes. The most typical flood-event of each hydrograph type was selected for morphodynamic modelling to evaluate the channels morphodynamic response and sediment transport dynamics. The flood-events extracted from the classified hydrographs were linked with climate data from equivalent time period to examine possible connections between climate and flood-event shapes. Mann-Kendall trend test was run on the hydroclimatic variables to detect possible trends in the time-series. Continuous discharge and water level monitoring has been conducted in Pulmanki River since 2008 during open water season (May-September). The Pulmanki River discharge time-series was complemented with Polmak discharge station data from Tana River (Fig. 1) to cover the whole 32-year time period. Sediment and bedload transport samples were collected during the spring and autumn field campaigns in 2019 from various discharge conditions.

3.1 Hydrograph measurements and generation

184 Hydrographs of open water season were generated utilising a combination of data sources.
185 For the years 2008-2023, rating curves based on a combination of field data were generated:
186 water pressure sensor data (Levellogger 5, Solinst), water level data measured with Virtual
187 Reference Station-Global Navigation Satellite System (VRS-GNSS), and discharge data
188 measured with Acoustic Doppler Current Profiler (ADCP M9, Sontek). Each year, the water
189 pressure sensors were placed into the upper Pulmanki River after ice-breakup in spring and
190 picked up before winter (see locations in Fig 1). This way the sensors covered the whole
191 open water season and seasonal variations of water pressure, water level and discharge
192 with 15 minute intervals. The location of the sensors was identical each year. To compensate
193 atmospheric influence on water pressure, an air pressure sensor data from Solinst
194 Barologger was subtracted from the water pressure readings. During field campaigns in May
195 and September water level and discharge were measured daily from the LeveLogger
196 locations for creating rating curves between LeveLogger pressure, water level (WL) and
197 discharge (Q). Based on the rating curves, a 3rd order polynomial function was selected for
198 calculating annual hydrographs of open water seasons (Figure 2A).

199

200 For the years 1992-2007, openly available daily discharge data from Polmak measurement
201 station, maintained by the Norwegian Water Resources and Energy Directorate (NVE) was
202 used. The station is located in the main channel of Tana River at the spot where Pulmanki
203 River discharges into Tana (see Fig. 1, Q station number 3), and has been operating since
204 November 1991. The discharge for Pulmanki River was derived from the Polmak station data
205 using rating curve and 3rd order polynomial function between the Polmak station discharge
206 (Q) and Pulmanki River Q of 2008-2023 derived from the LeveLoggers (Figure 2B). Note
207 that the discharge of the Tana River continues to rise even as the discharge of the Pulmanki
208 River decreases, owing to the fact that the Tana River drains a catchment area 20 times
209 larger than that of the Pulmanki River. The Pulmanki River catchment (a sub-catchment of
210 the Tana) is situated approximately 200 km downstream from the Tana River headwaters
211 and lies in much lower terrain (with a maximum elevation of 400 m above sea level),
212 compared to the Tana catchment, which includes areas reaching up to 1,100 m above sea
213 level. This results in a delay in snowmelt, causing peak runoff in the Tana River to occur later
214 than in the Pulmanki catchment. The final hydrographs of Pulmanki river are based on these
215 two equations and data sources. The hydrographs were validated against ADCP discharge
216 measurements from Pulmanki River main channel. These measurements were excluded
217 from the rating curve creation. See the details of error metrics in Table 1.

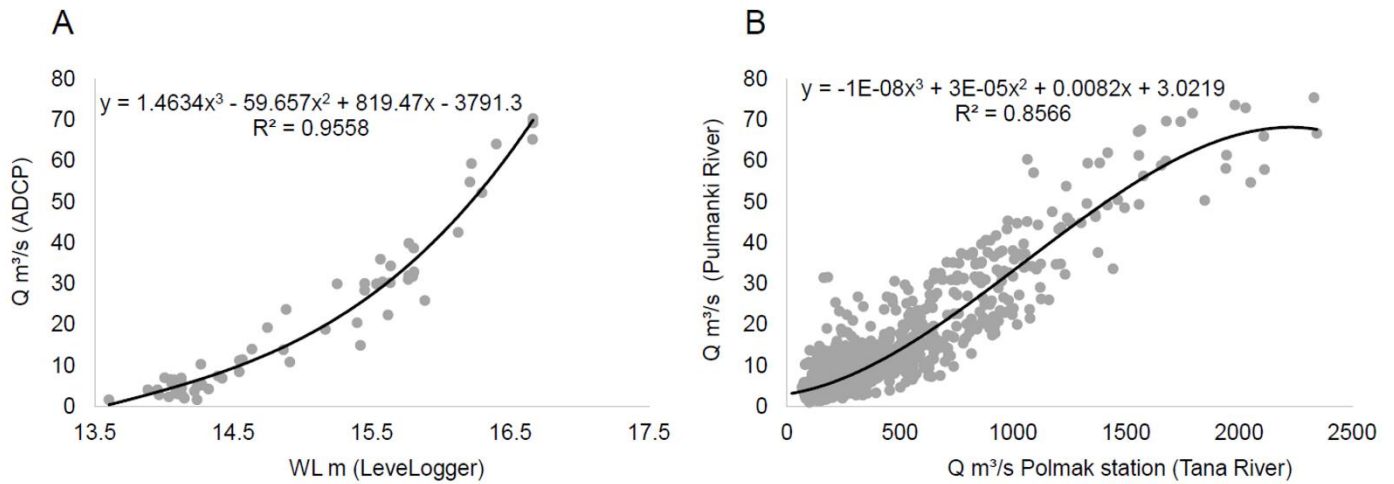


Figure 2. Rating curves for Pulmanki River hydrographs. A) Regression curve of discharge measurements ($Q \text{ m}^3/\text{s}$ ADCP) and LeveLogger water level (WL) in Pulmanki River 2008-2023. This polynomial function A was used to calculate hydrographs for years 2008-2023 B) Regression curve showing the relationship between the discharge in Pulmanki ($Q \text{ m}^3/\text{s}$ calculated based on regression curve A) and Polmak ($Q \text{ m}^3/\text{s}$ measured, national gauging station) during 2008-2023. This polynomial function B was used for calculating Pulmanki River discharge for years 1992-2007.

Table 1. Error metrics of the final hydrographs derived from two different data sources: LeveLogger discharge data and Polmak Station discharge data. MAE = Mean Absolute Error, SDE = Standard Deviation of Error, r = Correlation Coefficient, n = Number of samples.

Pulmanki River Q Derived from:	Min. Error (m^3/s)	Max. Error (m^3/s)	Mean Error (m^3/s)	MAE (m^3/s)	SDE (m^3/s)	r	R^2	n
LeveLogger	-9.59	10.73	-0.24	2.92	3.74	0.94	0.89	152
Polmak Station	-51.48	20.34	-0.39	2.59	4.65	0.89	0.80	1804

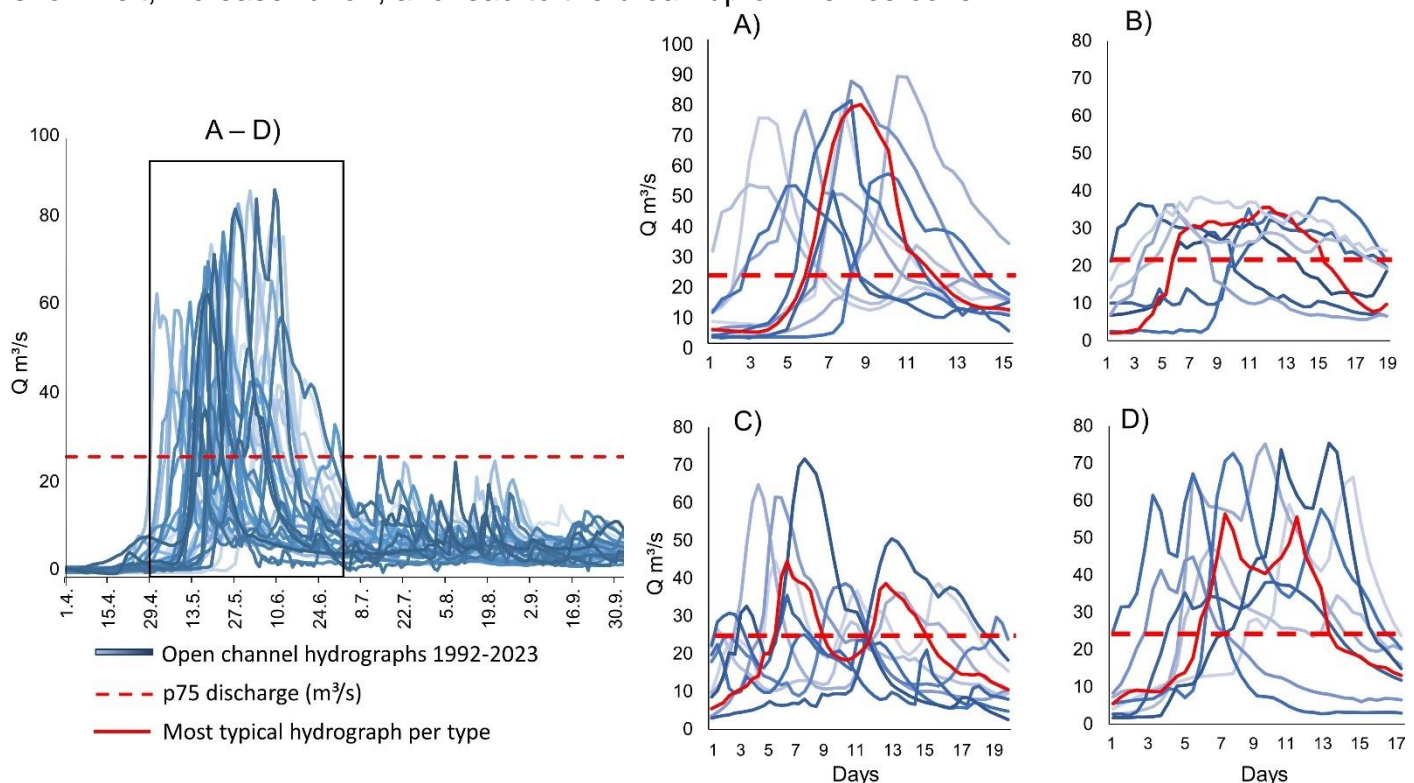
3.2. Hydrograph classification

The hydrographs were classified into distinct flood-event types based on the peak shape in Python program using the SciPy Scientific Python (SciPy) library. A threshold value of $23.46 \text{ m}^3/\text{s}$ (75th percentile, p75 discharge) for flooding was set to classify significant spring flood-events. A sensitivity analysis on peak-finding thresholds was conducted using the 50th, 60th, 70th, 80th, and 90th percentiles. Threshold values at the 70th and 80th percentiles were found to capture the majority of relevant spring flood events, and consequently, the 75th percentile (p75) was selected for this study. The commonly used threshold of the 90th percentile ($Q > 58 \text{ m}^3/\text{s}$ in this case) restricted the dataset too severely, with the algorithm failing to detect spring floods in certain years, particularly those with low peak discharges. Furthermore, using the p90 value resulted in hydrographs that included only the very peak of the flood event, without capturing the rising and falling limbs of the hydrograph, which are crucial for evaluating sediment dynamics and flow–sediment interactions. Thresholds below

the 70th percentile included peaks outside of spring flood season, and thus these thresholds were not ideal for this study. The definition for high and low flood-event was set to be either above or below the mean flood discharge of 40 m³/s, respectively.

The event classification was done by estimating different flood peak features such as peak timing, prominence, peak height, and event duration. First, a Savitzky-Golay smoothing filter was applied to the dataset to reduce noise and enhance the detectability of flood peaks. This was accomplished using the Savgol_filter function from the `scipy.signal` module, with a window size of 11 and a polynomial order of 3 to preserve relevant hydrograph features. Peak shapes within the smoothed data were identified and classified into distinct flood-events using the `find_peaks` function from the `scipy.signal` module. The following parameters and minimum values were found to most effectively identify peak events: the minimum discharge threshold for a flood event, defined as the 75th percentile (p75 Q), a minimum hydrograph width of one day, measured from the start of the rising limb to the end of the recession limb, and a minimum prominence of 2 m³/s, indicating how much the peak stands out from the surrounding baseline.

Four different event types were detected: A) High one-peak ($Q > 40$ m³/s), B) Low one-peak ($Q < 40$ m³/s), C) Two separate peaks ($Q > p75$, $Q < p75$, $Q > p75$), and D) Wavy peak (two $Q > p75$ peaks) (Figure 3A-D). For modelling purposes, the most typical event of each type was selected (red solid line in Fig. 3A-D). The precipitation-driven discharge peaks in July, August and September were left out of the analysis as none of them exceed the flood threshold discharge of p75. In addition, previous studies indicate that the majority of high-latitude rivers transport most of their annual sediment load during the main flood event, namely the spring flood (Syvitski, 2002; Zhang et al., 2022; Blåfield et al., 2024b). Therefore, the focus of this study was placed solely on spring flood peaks. In this region, spring flood peaks are driven by climatic factors such as rising temperatures and rainfall, which induce snowmelt, increase runoff, and lead to the break-up of river ice cover.



272 Figure 3. All the generated hydrographs of years 1992-2023. The classification led to four
273 distinct flood-event shapes: A) High one-peak flood, B) Low one-peak flood, C) Flood with
274 two separate peaks, and D) Flood with a wavy peak. The solid red hydrograph is the most
275 typical flood-event of each shape which was thus used in the morphodynamic model. Red
276 dashed line is the 75th percentile threshold discharge for spring flood.

277 3.3. Hydroclimatic data and statistical analysis

278 Climate data from the Nuorgam weather station (see location in Fig. 1B), 11 metres above
279 the mean sea level and 17 kilometres North from the Pulmanki River study area, was
280 downloaded from the Finnish Meteorological Institutes open data service. Daily Total, Min,
281 Mean and Max temperature, precipitation, and snow depth data of years 1991-2023 were
282 selected for the variance and trend analysis as these variables are closely related to the
283 hydrological properties of rivers (Veijalainen et al., 2010; Irannezhad et al., 2022). Annual
284 Min, Mean, Max and Total values were derived from the daily data and used in the trend
285 analysis (Fig. 4). In addition, duration of snow cover, number of precipitation-days, and
286 occurrence of extreme snow/precipitation events (95th percentile) were derived for the trend
287 analysis. For detailed analysis of springtime trends, the corresponding measures were
288 derived for March, April, and May as well. Only one weather station was included in the
289 analysis as other stations are located 50-100 kilometres away with over 100-meter elevation
290 difference to the area of interest. The year 1991 was included in the climate time-series as
291 the analysis was conducted on hydrological years instead of calendar years.

292 The Mann-Kendall (M-K) trend test was carried out on all climate variables with $\alpha = 0.05$
293 significance level to identify statistically significant monotonic trends. In addition to climate
294 variables, the MK-trend test was run on the classified flood hydrographs to examine trends
295 in the occurrence, timing, volume, and duration of each flood-event hydrograph type.
296 Possible serial correlations were removed by using Hamed & Rao (1998) M-K modification
297 which is explained in detail in e.g., Daneshvar Vousoughi et al., (2013) and in Jhajharia et
298 al., (2014). The effect of outliers on the trend was removed by using a non-parametric linear
299 regression Sen's slope estimator (Sen, 1968). Analysis of Variance (ANOVA) with $\alpha = 0.05$
300 significance level was run to identify possible significant differences between the means of
301 the variables, i.e. whether the annual/cold-season/spring or May weather conditions differ
302 significantly across the four spring flood-event type.

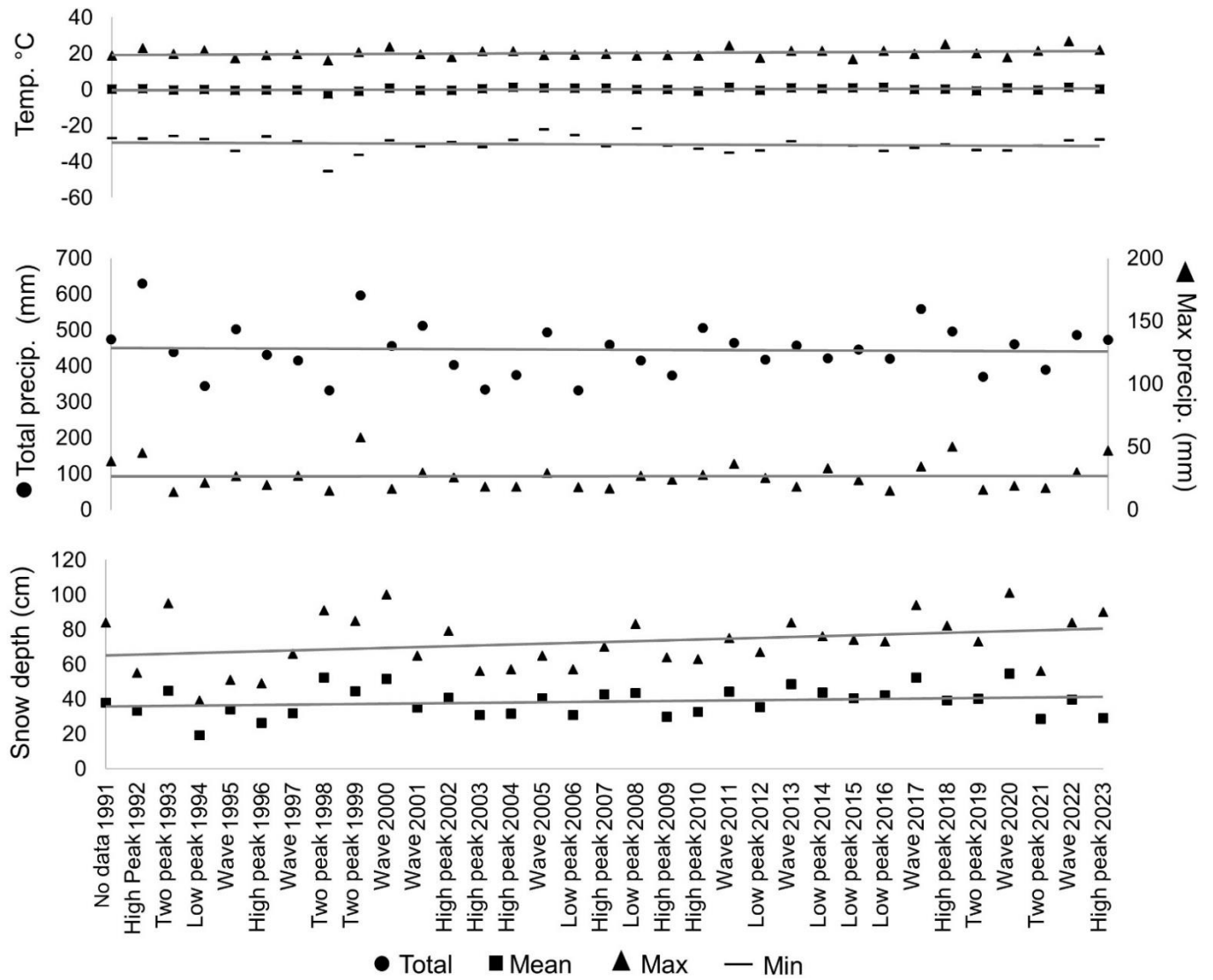


Figure 4. The annual climate time-series of the 32-year time period derived from the daily data. The corresponding flood-event types are marked on the x-axis.

3.4. Sediment and bedload sampling

Both grab samples with Van Veen sediment sampler, and bedload samples with Helley-Smith sampler were collected from the riverbed in 2019. A total of 70 grab samples (ca. 500 g) and 24 bedload transport samples were collected during various discharges from the area of interest. Grab samples were collected across the entire 6-kilometre reach during a single autumn field campaign under low discharge ($4.2 \text{ m}^3/\text{s}$) conditions. Samples were taken from the channel bed at left and right bank of each meander inlet, apex and outlet. Bedload transport samples were obtained during both, spring and autumn campaigns, under varying discharge levels ($7.5 \text{ m}^3/\text{s}$, $56 \text{ m}^3/\text{s}$, and $4.2 \text{ m}^3/\text{s}$). Twelve bedload transport samples were collected per campaign, each with a sampling duration of six minutes. The samples were dry sieved using half-phi intervals and the amount of material in each sieve was weighted. Sample statistics were calculated in GRADISTAT-program (Blott & Pye, 2010) using the Method of Moments which is based on a logarithmic distribution of sample phi sizes. GRADISTAT utilises its own scale with only four classes (Silt, $0.002\text{--}0.063 \text{ mm}$, Sand,

0.063–2 mm, Gravel, 2–64 mm and Boulders 64–2048 mm). The results of sediment and bedload sampling were utilised in the morphodynamic model as multiple sediment fractions, spatially varying Manning’s Roughness parameter, and for calibrating and validating the sediment transport rates (see details in Blåfield et al., 2024b).

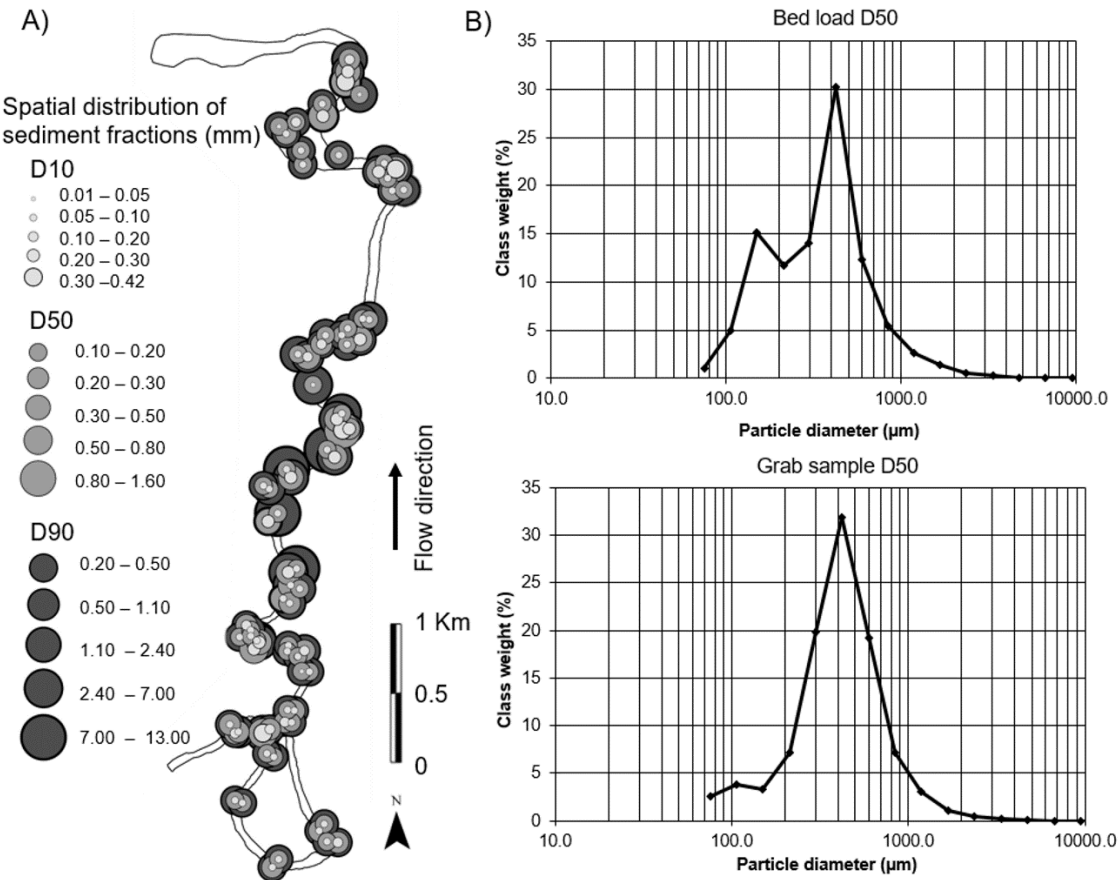


Figure 5. A) Spatial distribution of sediment fractions D10, D50 and D90 based on the collected field samples. B) D50 particle diameter distribution of all the collected bedload and grab samples in micrometres.

3.4 Morphodynamic modelling

The authors have previously presented and validated the model used in this study (Blåfield et al., 2024b). In this study, four distinct flood-event hydrographs (A-D in Table 2.) were simulated using the same initial channel geometry and sediment composition. A depth-averaged morphodynamic model with curvilinear, unstructured grid of 2x2 meter cell size was built utilizing FLOW 2D-module of Delft3D software. The model geometry was based on a digital elevation model derived from Structure-from-Motion (SfM). Specific details of the SfM creation can be found in Blåfield et al., (2024b), and general from Micheletti et al., (2013), and Dietrich et al., (2017). Multiple sediment fractions and spatially varying Manning's Roughness based on the grab sediment samples from the field were used, as these additions have been shown to significantly improve predicted morphodynamics (Kasvi et al., 2014). Each simulation featured hourly varying discharge conditions to evaluate sediment transport dynamics, sediment transport hysteresis patterns, and morphological responses to the shape and sequencing of the simulated hydrographs. The model time-step

344 was set to 0.05 minutes, with both spin-up and output intervals set at 720 minutes.
345 Morphology, source and sink terms, and total sediment transport were updated at each time
346 step. The model solved morphology independently based on the source and sink terms of
347 van Rijn (1993) approach. Transport boundary conditions, i.e., sediment feeding into the
348 model, were solved using the Neumann law and updated at each time-step. This allowed
349 the model to dynamically adjust the sediment supply and concentration at the inflow to match
350 the internal model conditions, thereby minimising accretion near the model boundaries.
351 Subsequently, sediment transport hysteresis and geomorphic activity for each flood-event
352 type were calculated from the source and sink terms, as well as from the modelled total
353 volume of sediment mobilised within the inundated area. The default scheme for dry-cell
354 erosion of banks was applied without further adjustment, as the focus of the study was on
355 longitudinal sediment transport and vertical changes to the channel bed. Detailed
356 parametrisation, as well as the model's calibration and validation are provided in Blåfield et
357 al., (2024b).

358 Delft3D is unable to simulate ice-covered flows or the effects of freeze–thaw processes on
359 bank erosion. These limitations, together with the absence of vertical flow representation in
360 the two-dimensional simulation, introduce simplifications into the modelling of flow dynamics
361 and sediment transport. The use of user-defined parameters further contributes to
362 uncertainty, particularly in the spatial and temporal patterns of erosion, transport, and
363 deposition. The van Rijn (1993) approach is sensitive to user-defined parameters such as
364 sediment fraction, composition, and associated threshold conditions (Pinto et al., 2006).
365 However, Kasvi et al. (2014) demonstrated that the van Rijn formulation performs more
366 reliably when applied with spatially variable, field-based sediment fractions and Manning's
367 roughness coefficients rather than uniform values. While the van Rijn transport formula
368 typically produces lower transport rates than other formulations (Schuurman et al., 2013;
369 Kasvi et al., 2014), it remains widely regarded as the most physically based and reliable
370 method (Pinto et al., 2006; Kasvi et al., 2014). The user-defined parametrisation used in the
371 present study is detailed in Blåfield et al. (2024b). Spatial variability in sediment grain size
372 and Manning's roughness, alongside the inclusion of medium transverse bed slope effects,
373 were identified as key parameters influencing sediment load predictions and morphological
374 change (Nicholas, 2013; Kasvi et al., 2014), and were prioritised for refinement during
375 simulation.

376 Table 2. The details of each model run. The flow conditions of flood-events A-D are based
377 on the hydrograph classification in section 3.2. The morphological parameters are based on
378 the sediment and bedload sampling from the field.

Event	Duration (days)	Peak Q m ³ /s	Total Q Volume m ³	Sediment Supply	Morphology	Sediment composition
A	7	80	29 868 586	Feeding	Sand bed	Sand, Gravel
B	13	35	34 851 505	Feeding	Sand bed	Sand, Gravel
C	14	48	26 2383 45	Feeding	Sand bed	Sand, Gravel
D	9	60	31 20 1609	Feeding	Sand bed	Sand, Gravel

379

380 4. Results

381 382 4.1 Hydroclimatic conditions and flood-event type variability

383 The variance analysis of flood events of types A–D and the prevailing climatic conditions
384 indicated that the climatic conditions of the preceding hydrological year were the most
385 significant of the tested variables influencing the type of spring flood event (Table 3). Other
386 significant factors influencing the flood-event type included the cold season (October–May)
387 mean temperature, spring rainfall (March–May), and May warmth, expressed as the
388 cumulative temperature sum in May (Table 3). In addition to climatic conditions, the timing
389 of peak discharge varied significantly between event types. The number of snow cover days
390 in May demonstrated a trend approaching statistical significance (Table 3). By contrast,
391 rainfall during the cold season, May rainfall, and the spring mean temperature did not exhibit
392 significant differences between flood-event types (Table 3).

393 Flood events of Type A were typically associated with high annual snow accumulation, low
394 annual temperatures, and rapid warming in May, resulting in a low number of snow cover
395 days during May (Fig. 6). These events also experienced high annual precipitation but low
396 spring rainfall (Fig. 6). Thus, flood events of Type A can be characterised as occurring in
397 cold, snow-rich years, where rapid warming in May leads to sharp and high flood
398 hydrographs. Flood events of Type B were associated with the warmest cold season mean
399 temperatures, along with moderate spring rainfall, snow accumulation, and cumulative May
400 temperatures (Fig. 6). These conditions suggest that snowmelt may begin during the cold
401 season and continue through spring, resulting in reduced energy availability during the main
402 melt period in May. Flood events of Type C were linked to the lowest annual precipitation,
403 the lowest cold season temperatures, and the coldest May temperatures (Fig. 6). However,
404 these events also exhibited the highest snow accumulation during spring. Overall, Type C
405 floods reflect dry, mixed, or transitional climatic conditions, in which a particularly cold winter
406 and spring lead to delayed snowmelt. This delayed melt, when combined with May rainfall
407 and variable temperatures, may result in two distinct melt peaks. Flood events of Type D
408 were characterised by high annual and spring snow accumulation, alongside the warmest
409 annual and cold season mean temperatures, but relatively low temperatures in May, leading
410 to a prolonged persistence of snow cover during May. These events also experienced high
411 annual precipitation and considerable variation in spring rainfall. Consequently, this flood
412 type typically occurs following a warm and wet year, when May is cold and experiences
413 highly variable rainfall, resulting in non-uniform snowmelt and the development of wavy
414 hydrographs.

415 Table 3. Results of one-way ANOVA test on the main variables with $\alpha = 0.05$ significance
416 level. Statistically significant p-values are bolded. T = Temperature, P = Precipitation, Cold
417 season = October-May, Spring = March, April, May.

Variable	F-statistics	p-Value
Annual mean T	3.73	0.022

Annual snow sum	7.73	0.006
Annual total P	4.00	0.017
Cold season mean T	3.38	0.032
Cold season Rainfall	2.26	0.104
Spring mean T	1.78	0.174
Spring snow sum	1.93	0.103
Spring rainfall	3.13	0.050
May cumulative T	3.41	0.032
May n. of snow cover days	2.36	0.083
May Rainfall	0.97	0.420
Peak Q timing	3.28	0.035

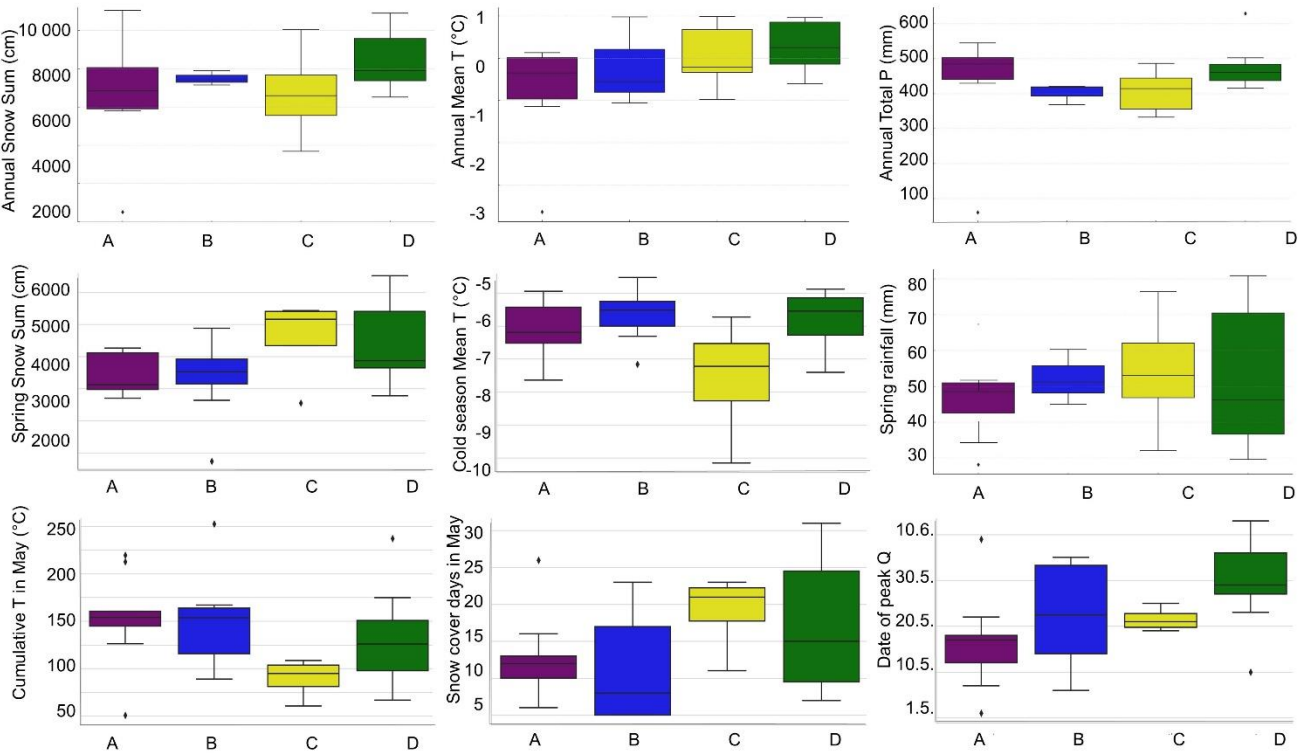
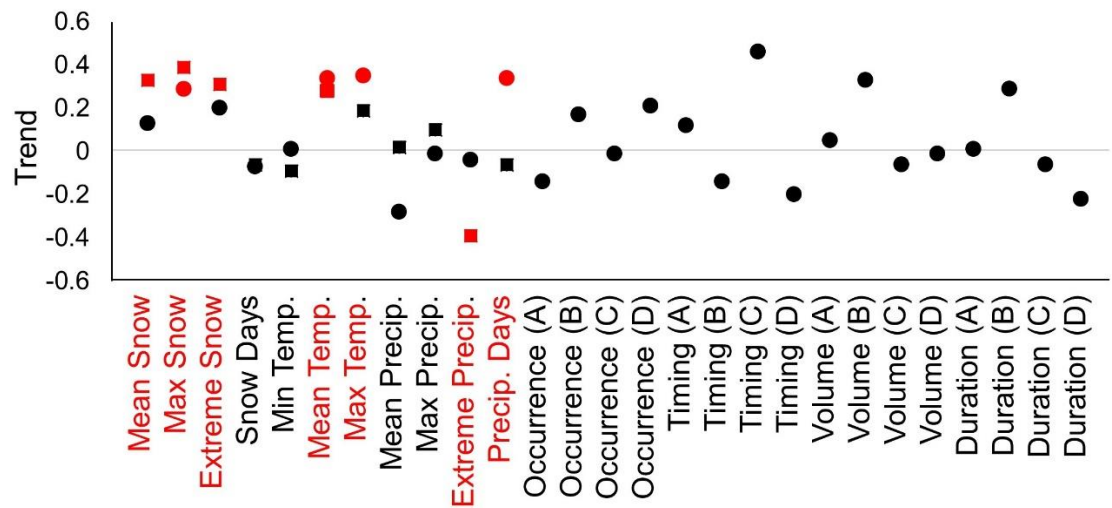


Figure 6. Statistically significant differences between the variable means illustrated in the boxplots, showing the distribution, median, and variation of climate variables associated with each flood-event type. Two borderline variables close to significance (May snow cover days and spring snow sum) were plotted as well.

The wavy (D) and high one-peak (A) events appeared the most frequently, both occurring 10 times within the 32-year time-series. The wavy events of type D had an average duration of 9 days whereas high one-peak event of type A lasted 7 days on average. Low one-peak events of type B occurred 7 times and had the longest average duration of 13 days. Finally, the two-peak events of type C were the least frequent type with only five occurrences lasting 14 days on average. No significant trends were observed in re-occurrence, duration, volume, or timing of any of the flood-event types within the 32-year time-series (Fig. 7). Trend analysis on the climate variables indicate that in snow-related variables (mean, maximum, and extreme snow), all annual trends (square marker) were positive with statistically significant

435 increase. The max snow amount had statistically significant trend also in spring (March-May,
 436 circle marker). The number of snow days, however, showed a non-significant weakly
 437 negative trend (Fig. 7). Temperature trends were mostly positive, with statistically significant
 438 increases in both annual and spring mean temperature (Fig. 7). Spring-time max
 439 temperature had significant increasing trend indicating that especially springs have gotten
 440 warmer over the time-series. Minimum temperature showed non-significant trend in annual
 441 and spring-time data. Precipitation-related trends were more variable. Mean and max
 442 precipitation exhibited mostly negative non-significant trends or no trend at all, while the
 443 annual extreme precipitation (95th percentile) showed significant decreasing trend (Fig.
 444 7). Even though the spring-time precipitation did not indicate significant trends in volume, the
 445 number of precipitation days had significant increasing trend.

446 Overall, the results suggest that while the frequency and characteristics of individual flood-
 447 event types have remained relatively stable over the 32-year period, underlying climatic
 448 drivers have undergone notable changes. In particular, the increase in snow accumulation
 449 and rising spring temperatures point toward a shift in the timing and dynamics of snowmelt,
 450 even if not yet reflected in observable flood trends. The significant rise in the number of
 451 precipitation days during spring, despite no clear trend in total precipitation volume, may also
 452 contribute to more fragmented or prolonged runoff events, potentially supporting the
 453 occurrence of events of type B and D.



454
 455 Figure 7. The M-K-trend test results of the climate-related variables during the 32-year study
 456 period. Red markers indicate statistically significant trends and black markers non-
 457 significant. Square markers represented annual trends, while circles represent seasonal
 458 trends in spring (March-May).

459 4.2 Morphological response to sediment transport hysteresis

460 The modelled results suggest that hydrograph shape may have a significant influence on
 461 morphological response and sediment transport hysteresis. Both the total transported
 462 sediment (TTS, calculated across the entire model area) and the type of sediment transport
 463 hysteresis appeared to vary across the modelled events. The wavy event (Type D) was
 464 associated with the largest volume of TTS, with the first peak contributing approximately
 465 59% and the second peak 41% of the event's TTS. Thus, the transport rate during the first
 466 peak was about 28% higher than during the second peak. In the flood event characterised

467 by two separate peaks (Type C), the first peak contributed 63% and the second 37% of the
468 total TTS. Consequently, the transport rate during the second peak was approximately 42%
469 lower than during the first. The TTS of event C was around 17% lower than that of event D.
470 The high one-peak event (Type A) yielded a TTS volume approximately 4% lower than event
471 D and about 11% higher than that of event C. In contrast, the low one-peak event (Type B)
472 exhibited a TTS volume about 30% lower than that of the high one-peak event (Type A), and
473 approximately 20–32% lower than the double-peaking events C and D, respectively.

474
475 All events predominantly exhibited counterclockwise sediment transport hysteresis, where
476 the transport peak occurred after the peak discharge (Fig. 8A–D), suggesting that sediment
477 transport lagged behind changes in discharge and flow conditions. However, the modelled
478 sediment transport hysteresis loops appeared to vary in complexity and shape depending
479 on the flood-event type.
480 The single-peak events (Types A and B) displayed relatively simple counterclockwise loop-
481 shaped hysteresis, with sediment transport following the peak discharge (Fig. 8A–B). Event
482 C appeared to exhibit a more complex hysteresis pattern, including multiple
483 counterclockwise loops, which may indicate that sediment mobilised during the first peak
484 was partially deposited between the peaks, as the second peak showed significantly lower
485 TTS (Fig. 8C). In the wavy event (Type D), the first peak exhibited counterclockwise
486 hysteresis, whereas sediment transport during the second peak appeared to precede the
487 second discharge peak, resulting in clockwise hysteresis (Fig. 8D). This complexity may
488 reflect variability in sediment mobilisation processes and sediment availability.
489 Across all events, higher TTS values were observed during the falling limb compared to the
490 rising limb at corresponding discharge values, suggesting that sediment transport was not
491 directly proportional to discharge (Fig. 8A–D). This discrepancy highlights the potential
492 influence of delayed and progressive sediment mobilisation, as well as the lagged
493 morphological response of bedforms. These findings imply that flood-event shape may have
494 a considerable influence on sediment transport hysteresis and, consequently, on riverbed
495 morphological development.

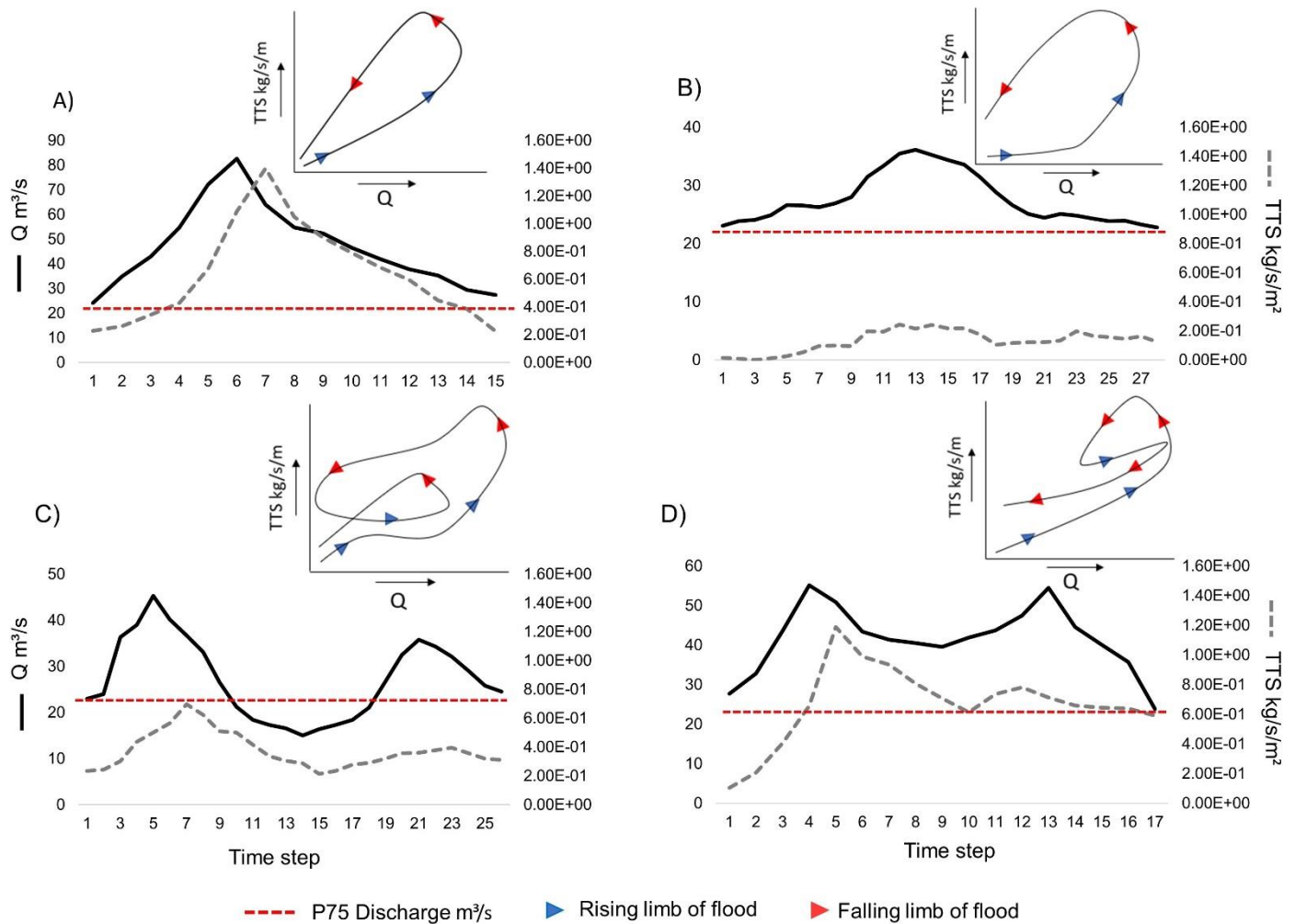
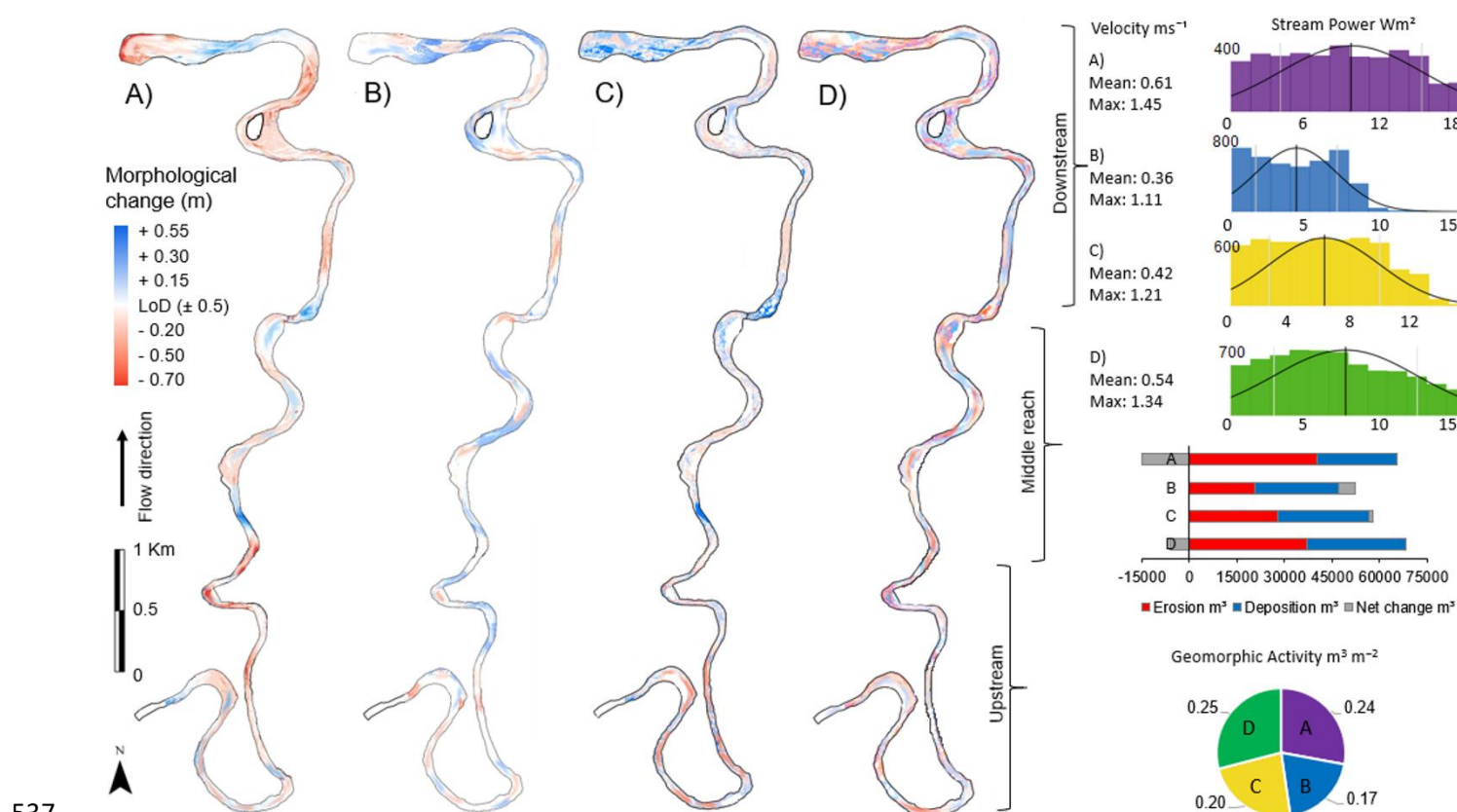


Figure 8. The modelled flood-event hydrographs and sediment load at each timestep. On the upper right corner of each graph is the sediment transport hysteresis of the event type. The blue arrows indicate rising limb and red arrows falling limb of the flood. The red dashed line shows the threshold p90 discharge. A) High one-peak event and sharp counterclockwise sediment transport hysteresis. B) Low one-peak event and wide counterclockwise sediment transport hysteresis. C) Event with two separate peaks and counterclockwise sediment transport hysteresis with a loop. D) Wavy type event and hysteresis loop with counterclockwise and clockwise directions.

Each modelled event appeared to demonstrate different patterns of morphological response (Fig. 9A–D), influenced by variations in sediment transport hysteresis, stream power, and flow velocity. Event A produced the second highest total volume of mobilised sediment and geomorphic activity (Fig. 9A). Based on the model, this event appeared to experience the most extensive erosion throughout the reach, with deposition areas remaining relatively localised. The highest stream power values were modelled in this event, exceeding 24 W/m^2 , alongside a mean flow velocity of 0.61 m/s , both of which likely contributed to substantial erosion and an overall net sediment loss of $-14,772 \text{ m}^3$. Sediment input from upstream was insufficient to compensate for this loss. In contrast, event B exhibited the lowest geomorphic activity, with a more balanced distribution of erosion and deposition across the river reach, resembling classical meander behaviour with distinct riffles and pools (Fig. 9B). Stream power during this event was considerably lower, predominantly below 10 W/m^2 , with a mean

517 flow velocity of 0.36 m/s. These conditions likely facilitated the deposition of eroded and
 518 transported sediment within the reach, resulting in a net sediment gain of 5,482 m³.

519 Event C showed a relatively balanced response, with an even distribution of erosion and
 520 deposition, and the smallest net change, resulting in a sediment gain of 1,132 m³ (Fig. 9C).
 521 The upstream section experienced the greatest erosion, while sediment accumulation was
 522 most pronounced downstream. Only minor changes occurred in the middle reach based on
 523 the model. Stream power for event C was moderate, with values mostly below 16 W/m² and
 524 only occasional exceedances above 20 W/m². Event D exhibited the most fragmented
 525 morphological response, with small, scattered areas of both erosion and deposition
 526 distributed throughout the reach (Fig. 9D). The stream power distribution for event D was
 527 more similar to that of event A, with values exceeding 20 W/m² and a mean flow velocity of
 528 0.54 m/s. Despite the relatively high energy, event D produced a more balanced sediment
 529 budget, though it still resulted in a net sediment loss of -6,267 m³. Geomorphic activity per
 530 unit area appeared highest for events A and D, both of which showed considerable sediment
 531 mobilisation but resulted in different morphological responses likely due to hydrograph
 532 shape. Events B and C exhibited lower geomorphic activity, with a tendency towards
 533 sediment deposition rather than erosion. The pattern of morphological change associated
 534 with the modelled flood events thus appeared to be linked to the peak shape, sequencing,
 535 and the resulting sediment transport hysteresis patterns, which collectively influenced the
 536 morphological response of bedforms.



537 Figure 9. Morphological adjustment of each flood-event (A-D) in left panel: A) Distinct areas
 538 of heavy erosion and deposition. B) Desecrate morphological changes but distinct areas of
 539 erosion and deposition. C) More complex morphological changes patched around the river
 540 reach. D) Heavy erosion and deposition spread complexly inside the reach. Right panel: A-
 541

542 D events mean and max velocity, histograms of stream power (x) distribution within number
543 of model cells (y), volume of erosion, deposition, and net change, and geomorphic activity.

544

545 **5. Discussion**

546

547 **5.1. Flood-event types and hydroclimatic conditions**

548 The results of variance analysis and trend test of climate variables and flood-event types
549 aligned with well-documented responses to climate change in cold regions (Cockburn &
550 Lamoureux, 2008; Vormoor et al., 2016; Matti et al., 2017; Arp et al., 2020). The significant
551 increase in both mean and maximum spring temperatures matched global climate model
552 predictions for continued warming at high-latitudes (Koenigk & Brodeau, 2017; Huo et al.,
553 2022). The increased snow depth also aligned with Pulliainen et al. (2020), who reported
554 rising snow accumulation and snow water equivalent (SWE) in the studied region. Despite
555 this, no significant changes in flood volumes were observed, consistent with previous studies
556 in Fennoscandia (Veijalainen et al., 2010; Korhonen & Kuusisto, 2010; Matti et al., 2017;
557 Lintunen et al., 2024). This lack of change was attributed to milder winter conditions and
558 longer snowmelt period resulting from warming temperatures, which lead to more stable
559 runoff during spring (Fischer & Schumann, 2019; Zhang et al., 2023). Additionally, no
560 significant trends were found in the timing, duration, or interval of flood-events, consistent
561 with earlier research in snowmelt-dominated regions (Veijalainen et al., 2010; Vormoor et
562 al., 2016; Matti et al., 2017).

563

564 Despite the absence of significant trends, low-peak floods (B) increased in both volume and
565 duration, while wavy floods (D) showed a reduction, respectively (Figure 7). Based on the
566 results of ANOVA, both flood-events of this type were influenced by high annual temperature
567 and high snow accumulation, but significantly different spring-time and May weather
568 conditions. Events of type B experienced long and warm melt period during spring whereas
569 events of type D were associated with late spring warmth with varying amounts of rainfall
570 leading to non-uniform runoff. The climatic conditions associated with these event types are
571 expected to intensify across the Northern Hemisphere (Callaghan et al., 2012; Kunkel et al.,
572 2016; Conolly et al., 2019; Pulliainen et al., 2020; Hu et al., 2023), although climate change
573 impact on snow accumulation is likely to vary spatially. These event types also exhibited an
574 increase of re-occurrence indicating that these flood-event types are likely to become more
575 common in the future. High one-peak floods (A), however, were associated with cold, snow-
576 rich years, where rapid warming in May leads to sharp and high flood hydrographs. This is
577 consistent with findings that cold springs delay snowmelt and ground thaw, leading to high
578 discharge peaks when the thaw eventually occurs (Labuhn et al., 2018). Unlike double-
579 peaking floods, single-peak events involved lower temperatures and rainfall during spring,
580 and therefore the rain-on-snow effect could be linked to the wetter conditions typical to
581 events of type D. Even though events of type C are also double peaking, these hydrographs
582 were linked to dry, mixed, or transitional climatic conditions, in which a particularly cold winter
583 and spring lead to delayed snowmelt. Hydrographs of event type C had however, significant

584 amount of rainfall in May which together with cold temperature conditions likely causes the
585 two separate melt peaks typical to this event.

586 Climate change is expected to increase annual temperatures and to modify the precipitation
587 patterns in high-latitude areas (Zhang et al., 2023; Blöschl et al., 2017). These changes will
588 likely have an impact on the occurrence of certain flood-event types. Increased spring rainfall
589 can increase rain-on-snow events significantly amplify runoff and flood peaks, particularly
590 together with deep snow packs and accelerated snowmelt from warmer spring
591 temperatures. Similar pattern have been recognized previously on high-latitudes by Fischer
592 & Schumann (2019). The results observed in this study point to the direction of possible
593 future hydroclimatic regime shift. These findings highlight the complex effects of climate
594 change on flood-events and underscore the importance of considering flood-event
595 sequencing in assessing the impacts of hydroclimatic shifts. Future research could explore
596 climate teleconnections, such as the North Atlantic Oscillation (NAO) or Arctic Oscillation
597 (AO), to better understand the conditions driving specific flood-events (Dahlke et al., 2012;
598 Villarini et al., 2013; Irannezhad et al., 2022). In addition, it is worth of noting that while
599 interpreting the results of this study, especially the results of ANOVA, the sample size has
600 a critical impact on the reliability and validity of the results. Larger sample sizes increase the
601 statistical power of the test, improving the ability to detect true differences between group
602 means (Lakens, 2022). They also provide more precise estimates of means and variances,
603 reduce the influence of outliers, and help satisfy the assumptions of normality and
604 homogeneity of variances. In contrast, small samples can result in underpowered tests,
605 unstable F-statistics, and greater sensitivity to assumption violations, ultimately reducing the
606 robustness of the findings

607

608 **5.2. Flood-event types and morphological response**

609 When interpreting the morphological results of the simulations in this study some limitations
610 should be considered. As a depth-averaged model, it did not resolve vertical flow structures
611 or secondary currents, which limit the capacity to fully represent sediment transport and bank
612 erosion processes (Pinto et al., 2006; Nicholas et al., 2014; Williams et al., 2014). In addition,
613 the model lacks the ability to simulate ice-covered flows and freeze-thaw effects, both of
614 which significantly influence sediment dynamics and channel stability in cold-region rivers
615 (Zhang et al., 2022). Model sensitivity to user-defined parameters, such as sediment
616 fractions and roughness coefficients, further contributes to output uncertainty (Pinto et al.,
617 2006). Moreover, the use of morphological acceleration factors and simplified boundary
618 conditions may exaggerate or underrepresent morphological processes. Consequently,
619 while the simulation runs presented in this study are effective in assessing relative
620 differences between scenarios, caution is necessary when interpreting absolute sediment
621 budgets and localised morphological changes due to simplifications, and the fact that it
622 cannot simulate ice and freeze-thaw effect on sediment transport and bank erosion. In
623 addition, only one hydrograph was modelled for each flood-event type, meaning that
624 selecting a different hydrograph of the same type could have resulted in different volumetric
625 changes and total amounts of transported sediment, as these depend on the flood's volume
626 and transport capacity. However, the findings of this study, together with previous laboratory
627 (Mao, 2012; 2018) and modelling studies (Kasvi et al., 2015), support the view that the shape

628 and sequence of the hydrograph play a crucial role in determining morphological outcomes.
629 Therefore, it is likely that selecting different hydrographs for each flood-event type would
630 have produced similar types of morphological patterns relative to the flood's magnitude and
631 transport capacity, even though the quantitative results may have differed.

632

633 Nevertheless, the model simulations showed that the channel bed's morphological response
634 was influenced by flood-event type and sequences, as well as sediment transport hysteresis
635 pattern, rather than just flood magnitude. Similar finding have been made by Kasvi (2015)
636 who found that the flood duration and flow characteristics have notable impact on channel
637 morphology. All events exhibited dominant counterclockwise hysteresis, common in sand-
638 bed rivers with upstream sediment supply and bedload-dominated transport (Tananev, 2015;
639 Gunsolus & Binns, 2017). However, the riverbed's morphological response varied depending
640 on the modelled hydrograph shape. Single-peak events (A and B) produced distinct erosion
641 and deposition patterns, while double-peaking events (C and D) led to fragmented, small-
642 scale morphological features. Particularly, event B formed classic riffles and pools, typical to
643 meandering rivers (Hooke, 2003, Salmela et al., 2022), whereas the reduced sediment
644 transport during second peaks in double-peaking events, also noted in previous flume
645 experiments (Martin & Jerolmack, 2013; Mao, 2018), resulted in more complex, small-scale
646 bedforms.

647

648 The reduction in sediment transport during the second flood peak has previously been linked
649 to bed surface reorganisation, notably the exposure of coarser material (armouring) and
650 infiltration of finer sediments (kinetic sieving), both of which stabilise the bed and increase
651 the energy required for sediment remobilisation (Curran & Waters, 2014; Dudill et al., 2017;
652 Ferdowsi et al., 2017; Mao, 2018). In contrast, event D displayed clockwise hysteresis during
653 the second peak, suggesting that the bed did not fully stabilise between peaks, enabling
654 more rapid sediment remobilisation and resulting in higher total transported sediment (TTS)
655 compared to other flood events. This pattern may also indicate increased input of finer
656 sediments from bank erosion, which tends to intensify during the falling limb of the
657 hydrograph as water levels decline (Lotsari et al., 2014; Lotsari et al., 2024; Yang et al.,
658 2024). Bank erosion dynamics are further influenced by freeze-thaw processes and the
659 presence of seasonally frozen ground, which the current model does not represent. The
660 thermal condition of banks and bars during different flood stages strongly affects erosion
661 rates, with thawed banks being considerably more erodible than frozen ones (Lotsari et al.,
662 2024; van Rooijen & Lotsari, 2024; Yang et al., 2024). Moreover, both soil moisture and the
663 number of freeze-thaw cycles reduce bank stability (Li et al., 2022; Lotsari et al., 2024). As
664 climate change is expected to prolong freeze-thaw periods (Blåfield et al., 2024a; Sha et al.,
665 2025), future bank erosion rates and sediment fluxes are likely to increase. Additionally,
666 enhanced cold-season discharge and earlier freshet onset under warmer conditions will
667 further promote riverbank erosion in many regions (Brown et al., 2020).

668

669 The fragmented bedforms from double-peaking floods were likely caused by secondary
670 bedforms cannibalizing the larger topography from the first peak, a phenomenon observed
671 in flume studies (Wilbers & Brinke, 2003; Martin et al., 2013). In addition to flood hydrograph

672 shape and hysteresis pattern, sediment particle size played a key role in morphological
673 adjustment. The middle reach with the largest particles (Fig. 5) was eroded mainly during
674 events A and D, while events B and C caused minimal change in this section of the river.
675 This finding was consistent with earlier research on particle size impact on sediment
676 transport hysteresis and remobilisation of the sediment particles (Mao, 2012; Malutta et al.,
677 2020). Despite variations in the modelled runoff volumes, the study identified distinct
678 morphological response patterns for each flood-event type. These patterns, shaped by
679 sediment transport hysteresis, distribution of sediment particle size and flood-event
680 sequences, align with findings from previous studies (Martin & Jerolmack, 2013; Gunsolus
681 & Binns, 2017; Mao, 2018). The results highlighted the crucial role of different flood-event
682 types in shaping river morphology, revealing that, while event variation likely helps maintain
683 channel equilibrium in long-term, prolonged exposure to certain events—such as high-
684 energy or multi-peaking floods—could disrupt this balance. Such evolution have the potential
685 to destabilise the channel, by altering sediment connectivity, transport processes, and
686 ultimately the morphological structure of the river systems (Bracken et al., 2015; Zhang et
687 al., 2023). Understanding these responses is essential for predicting future river behaviour
688 and managing morphological stability.

689

690 **5.3. Forecasted hydroclimatic shift and long-term morphological adjustment**

691 This study highlighted the importance of understanding how fluvial sand and gravel-bed
692 systems respond to climatic conditions, particularly by examining the sequences of flood
693 hydrographs, which are often overlooked, and more focus is paid on factors like flood
694 volume, timing, or frequency. The results revealed that flood-event type and peak
695 sequencing had significant impact on the morphological response of the channel. This
696 together with the observed trends, suggested that even in regions, like the one studied,
697 where hydroclimatic changes are not yet fully visible (Veijalainen et al., 2010; Lintunen et al.,
698 2024), flood-event characteristics are evolving with consequences to the river morphology.
699 This and the overserved trends in the hydroclimatic variables underscores that hydroclimatic
700 change is not uniform in space and time across cold regions and rivers should be assessed
701 at the catchment scale to predict future morphological adjustment accurately.

702

703 The increase (decrease) of double (single) peaking floods could lead to changes in river
704 system stability, sediment loads, and in the spatial distribution of long-term morphological
705 adjustment if certain type of morphological response begin to accumulate (Bracken et al.,
706 2015; Zhang et al., 2023; Blåfield et al., 2024a). Furthermore, previous research findings
707 suggesting that sediment loads in cold regions could rise by 20-30 % for every 1-2 °C
708 increase in temperature (Syvitski et al., 2002; Li et al., 2021) was supported by this study,
709 as the double-peaking floods related to warmer annual temperatures, showed higher
710 geomorphic activity and sediment loads compared to single peaking events of similar
711 volume. The temperature increase together with altered morphological response pattern
712 could eventually lead to sediment transport regime shift. However, the anticipated shift is
713 likely to be a gradual process (Zhang et al., 2023), and the river system may eventually
714 stabilise again. Yet, before stabilizing the shift is likely to challenge the river channel stability,

715 making the long-term morphological adjustment, like meander migration, less predictable
716 (Wohl et al., 2017; Hopwood et al., 2021).

717

718 Shifts in the sediment transport regime, along with changes in morphological response and
719 long-term adjustment to evolving flood patterns, are likely to influence the morphological
720 response to summer and autumn precipitation by altering sediment availability and bed form
721 composition. Although these precipitation peaks were not the focus of this study, these
722 seasonal peaks should be considered when predicting and evaluating long-term
723 morphological adjustment of river channels as the distribution of seasonal sediment load is
724 likely shifting towards summer and autumn peaks (Li et al., 2021; Zhang et al., 2023; Blåfield
725 et al., 2024a). This could have significant implications for river ecosystems, flood risk
726 management, and infrastructure planning (Beel., et al., 2021; Gupta et al., 2021; Najafi et
727 al., 2021). As discharge regimes become increasingly event-driven rather than seasonally
728 predictable, traditional models of sediment flux that assume clear seasonal patterns may no
729 longer be applicable. Hysteresis patterns, where sediment concentration and water
730 discharge are no longer linearly related, can reveal critical thresholds, sediment sources,
731 and system memory that are key to predicting future river behaviour. Therefore, future
732 research should focus on understanding the combined effects of flood-event sequencing,
733 changing precipitation patterns, and sediment transport dynamics under evolving climatic
734 conditions. Long-term monitoring and advanced modelling efforts will be essential to predict
735 the future morphological adjustments of rivers and develop strategies for mitigating these
736 changes' impacts on ecological systems.

737

738 **6. Conclusions**

739

740 The findings of this study emphasise the critical role that flood-event variability and
741 sequencing play in shaping the morphological response of fluvial sand and gravel-bed
742 systems in cold regions. The results demonstrated that even in areas where hydroclimatic
743 changes are not yet fully visible, flood-event characteristics are evolving and remain closely
744 linked to specific climatic conditions. Each flood-event type produced distinct morphological
745 responses, such as the formation of riffles and pools during single-peaking floods, and more
746 fragmented and irregular bed forms in double-peaking floods. Additionally, sediment grain
747 size significantly influenced the spatial distribution of erosion and deposition. The increase
748 of double-peaking flood-events, coupled with rising temperatures, could lead to a shift in
749 sediment transport regimes, resulting in heightened geomorphic activity and altered
750 sediment loads. The results underscore the importance of assessing hydroclimatic
751 conditions and flood hydrograph sequences at the catchment scale to accurately predict
752 future morphological adjustment as the impacts of hydroclimatic shift are not uniform across
753 the arctic. Future research should focus on the combined impacts of flood sequences,
754 precipitation patterns, and sediment transport dynamics to develop effective strategies for
755 managing the evolving river systems under climate change. These changes are expected
756 to affect long-term river stability, with significant implications for river ecosystems and flood
757 risk management.

758

759 **Data availability**

760 The climate data is openly available on Finnish Meteorological Institutes (FMI) data service.
761 The Polmak discharge station data is openly available on Norwegian Water Resources and
762 Energy Directorate (NVE) data service. All the other data is available on request.

763

764 **Author contribution**

765 Linnea Blåfield – Writing the manuscript, Field work, Methodology, Formal analysis,
766 Visualisation, Funding.

767 Carlos Gonzales-Inca – Formal analysis, Editing the manuscript

768 Petteri Alho – Field work, Data curation, Resources, Reviewing the manuscript, Funding,
769 Supervision

770 Elina Kasvi – Field work, Reviewing the manuscript, Funding, Supervision

771

772 **Declaration of competing interest**

773 The authors declare that they have no conflict of interest.

774

775 **Funding**

776 This study was funded by the Kone Foundation (202104246), AnthroCliMocs (355018), and
777 by the European Union's Next Generation EU recovery instrument (RRF) through the
778 Research Council of Finland projects: HYDRO-RDI-Network (337279), Green-Digi-Basin
779 (347701), and HYDRO-RI-platform (346161). The study received support also from the
780 Flagship Programme funding granted by the Research Council of Finland for Digital Waters
781 – DIWA Flagship (359247).

782

783 **Acknowledgements**

784 The authors would like to thank research assistant Oona Oksanen from the Fluvial and
785 Coastal Research Group (University of Turku) for helping with the data processing, and
786 other group members who have participated in the field work.

787

788

789 **References**

790 Arp, C. D., Whitman, M. S., Kemnitz, R., & Stuefer, S. L.: Evidence of hydrological
791 intensification and regime change from northern Alaskan watershed runoff.
792 Geophysical Research Letters, 47(17), e2020GL089186.
793 <https://doi.org/10.1029/2020GL089186>, 2020.

794 Beel, C. R, et al.: Emerging dominance of summer rainfall driving High Arctic terrestrial-
795 aquatic connectivity. Nat. Commun. 12, 1448 [https://doi.org/10.1038/s41467-021-](https://doi.org/10.1038/s41467-021-21759-3)
796 21759-3, 2021

797 Blåfield, L., Marttila, H., Kasvi, E., & Alho, P.: Temporal shift of hydroclimatic regime and its
798 influence on migration of a high latitude meandering river. Journal of Hydrology, 633,
799 130935. <https://doi.org/10.1016/j.jhydrol.2024.130935>, 2024a.

800 Blåfield, L., Calle, M., Kasvi, E., & Alho, P.: Modelling seasonal variation of sediment
801 connectivity and its interplay with river forms. Geomorphology, 463, 109346.
802 <https://doi.org/10.1016/j.geomorph.2024.109346>, 2024b.

803 Blöschl, G et al.: Changing climate shifts timing of European floods. Science 357, 588-
804 590(2017). DOI:10.1126/science.aan2506, 2017.

805 Bracken, L. J., Turnbull, L., Wainwright, J., & Bogaart, P.: Sediment connectivity: a
806 framework for understanding sediment transfer at multiple scales. Earth surface
807 processes and landforms, 40(2), 177-188. <https://doi.org/10.1002/esp.3635>, 2015.

808 Brown, D.R.N., Brinkman, T.J., Bolton, W.R. et al. Implications of climate variability and
809 changing seasonal hydrology for subarctic riverbank erosion. Climatic Change 162,
810 1–20, <https://doi.org/10.1007/s10584-020-02748-9>, 2020.

811 Callaghan, T.V., Johansson, M., Brown, R.D. et al.: The Changing Face of Arctic Snow
812 Cover: A Synthesis of Observed and Projected Changes. AMBIO 40 (Suppl 1), 17–
813 31. <https://doi.org/10.1007/s13280-011-0212-y>, 2011.

814 Cockburn, J. M., & Lamoureux, S. F.: Hydroclimate controls over seasonal sediment yield
815 in two adjacent High Arctic watersheds. Hydrological Processes: An International
816 Journal, 22(12), 2013-2027. <https://doi.org/10.1002/hyp.6798>, 2008.

817 Connolly R 1, Connolly M, Soon W, Legates DR, Cionco RG, Velasco Herrera VM. Northern
818 Hemisphere Snow-Cover Trends (1967–2018): A Comparison between Climate
819 Models and Observations. Geosciences. 9(3):135.
820 <https://doi.org/10.3390/geosciences90301>, 2019.

821 Curran, J. C., Waters, K. A., & Cannatelli, K. M.: Real time measurements of sediment
822 transport and bed morphology during channel altering flow and sediment transport
823 events. Geomorphology, 244, 169-179.,
824 <https://doi.org/10.1016/j.geomorph.2015.03.009>, 2015.

825 Daneshvar Vousoughi, F., Dinpashoh, Y., Aalami, M.T., Jhajharia ,D.: Trend analysis of
826 groundwater using non-parametric methods (case study: Ardabil plain) Stochastic
827 Environ. Res. Rsk Assessm., 27 (2013), pp. 547-559, DOI: 10.1007/s00477-012-
828 0599-4, 2013.

829 Fischer, S., Schumann, A.: Spatio-temporal consideration of the impact of flood-event types
830 on flood statistic. Stoch Environ Res Risk Assess 34, 1331–1351,
831 <https://doi.org/10.1007/s00477-019-01690-2>, 2020

832 Gaál, L. J.Szolgay, S.Kohnová, J.Parajka, R.Merz, A.Viglione, and G.Blöschl: Flood
833 timescales: Understanding the interplay of climate and catchment processes through
834 comparative hydrology, Water Resour. Res. 48, W04511,
835 <https://doi.org/10.1029/2011WR011509>, 2012

836 Gohari, A., Shahrood, A. J., Ghadimi, S., Alborz, M., Patro, E. R., Klöve, B., & Haghighi, A.
837 T.: A century of variations in extreme flow across Finnish rivers. *Environmental*
838 *Research Letters*, 17(12), 124027. DOI: 10.1088/1748-9326/aca554, 2022.

839 Gunsolus EH, Binns AD. Effect of morphologic and hydraulic factors on hysteresis of
840 sediment transport rates in alluvial streams. *River Res Applic.* 2018; 34: 183–192.
841 <https://doi.org/10.1007/s11356-021-16811-0>, 2022.

842 Gupta, H., Reddy, K.K., Gandla, V. et al. Freshwater discharge from the large and coastal
843 peninsular rivers of India: A reassessment for sustainable water management.
844 *Environ Sci Pollut Res* 29, 14400–14417, [https://doi.org/10.1007/s11356-021-16811-](https://doi.org/10.1007/s11356-021-16811-0)
845 [0](https://doi.org/10.1007/s11356-021-16811-0), 2022.

846 Hamed, K. H., & Rao, A. R.: A modified Mann-Kendall trend test for autocorrelated data.
847 *Journal of hydrology*, 204(1-4), 182-196. [https://doi.org/10.1016/S0022-](https://doi.org/10.1016/S0022-1694(97)00125-X)
848 [1694\(97\)00125-X](https://doi.org/10.1016/S0022-1694(97)00125-X), 1998.

849 Hirvas, H., Lagerbäck, R., Mäkinen, K., Nenonen, K., Olsen, L., Rodhe, L., & Thoresen, M.
850 (1988). The Nordkalott Project: studies of Quaternary geology in northern
851 Fennoscandia. *Boreas*, 17(4), 431-437. [https://doi.org/10.1111/j.1502-](https://doi.org/10.1111/j.1502-3885.1988.tb00560.x)
852 [3885.1988.tb00560.x](https://doi.org/10.1111/j.1502-3885.1988.tb00560.x), 1988.

853 Hopwood, M.J., Carroll, D., Browning, T.J. et al.: Non-linear response of summertime marine
854 productivity to increased meltwater discharge around Greenland. *Nat Commun* 9,
855 3256, <https://doi.org/10.1038/s41467-018-05488-8>, 2018.

856 Hooke, J.: River meander behaviour and instability: a framework for analysis. *Transactions*
857 *of the Institute of British Geographers*, 28(2), 238-253. [https://doi.org/10.1111/1475-](https://doi.org/10.1111/1475-5661.00089)
858 [5661.00089](https://doi.org/10.1111/1475-5661.00089), 2003.

859 Huo, R., Li, L., Engeland, K., Xu, C. Y., Chen, H., Paasche, Ø., & Guo, S.: Changing flood
860 dynamics in Norway since the last millennium and to the end of the 21st century.
861 *Journal of Hydrology*, 613, 128331. <https://doi.org/10.1016/j.jhydrol.2022.128331>,
862 2022.

863 Hu, Y., Che, T., Dai, L., Zhu, Y., Xiao, L., Deng, J., & Li, X.: A long-term daily gridded snow
864 depth dataset for the Northern Hemisphere from 1980 to 2019 based on machine
865 learning. *Big Earth Data*, 8(2), 274–301.
866 <https://doi.org/10.1080/20964471.2023.2177435>, 2024.

867 Huss, B. Bookhagen, C. Huggel, D. Jacobsen, R. S. Bradley, J. J. Clague, M. Vuille, W.
868 Buytaert, D. R. Cayan, G. Greenwood, B. G. Mark, A. M. Milner, R. Weingartner, M.
869 Winder, Toward mountains without permanent snow and ice. *Earths Future* 5, 418–
870 435, <https://doi.org/10.1002/2016EF000514>, 2017

871 Irannezhad, M., Ahmadian, S., Sadeqi, A., Minaei, M., Ahmadi, B., & Marttila, H. (2022).
872 Peak spring flood discharge magnitude and timing in natural rivers across northern
873 Finland: Long-term variability, trends, and links to climate teleconnections. *Water*,
874 14(8), 1312. <https://doi.org/10.3390/w14081312>, 2022.

875 Jhajharia, D., Dinpashoh, Y., Kahya, E., Choudhary, R. R., & Singh, V. P. (2014). Trends in
876 temperature over Godavari River basin in Southern Peninsular India. *International*
877 *Journal of Climatology*, 34(5). DOI: 10.1002/joc.3761, 2014.

878 Johansson, P.: Late Weichselian deglaciation in Finnish Lapland. *Applied Quaternary*
879 *research in the central part of glaciated terrain*, 47, 2007.

880 Kasvi, E., Alho, P., Lotsari, E., Wang, Y., Kukko, A., Hyyppä, H., & Hyyppä, J.: Two-
881 dimensional and three-dimensional computational models in hydrodynamic and

882 morphodynamic reconstructions of a river bend: sensitivity and functionality.
883 Hydrological processes, 29(6), 1604-1629. <https://doi.org/10.1002/hyp.10277>, 2015.

884 Karimae Tabarestani, M., Zarrati, A.R.: Sediment transport during flood-event: a review.
885 Int. J. Environ. Sci. Technol. 12, 775–788, [https://doi.org/10.1007/s13762-014-0689-](https://doi.org/10.1007/s13762-014-0689-6)
886 6, 2015.

887 Kociuba, W.: The Role of Bedload Transport in the Development of a Proglacial River
888 Alluvial Fan (Case Study: Scott River, Southwest Svalbard). Hydrology, 8(4), 173.
889 <https://doi.org/10.3390/hydrology8040173>, 2021.

890 Korhonen, J., & Kuusisto, E.: Long-term changes in the discharge regime in Finland.
891 Hydrology Research, 41(3-4), 253-268. <https://doi.org/10.2166/nh.2010.112>, 2010.

892 Kunkel, K.E., Robinson, D.A., Champion, S. et al. Trends and Extremes in Northern
893 Hemisphere Snow Characteristics. Curr Clim Change Rep 2, 65–73,
894 <https://doi.org/10.1007/s40641-016-0036-8>, 2016.

895 Labuhn, I., Hammarlund, D., Chapron, E., Czymzik, M., Dumoulin, J. P., Nilsson, A., ... &
896 Von Grafenstein, U.: Holocene hydroclimate variability in central Scandinavia inferred
897 from flood layers in contourite drift deposits in Lake Storsjön. Quaternary, 1(1), 2.
898 2018.

899 Lakens, D.: Sample size justification. Collabra: Psychology, 8(1), 33267.
900 <https://doi.org/10.1525/collabra.33267>, 2022.

901 Li, C., Yang, Z., Shen, H. T., & Mou, X.: Freeze-Thaw Effect on Riverbank Stability. Water,
902 14(16), 2479. <https://doi.org/10.3390/w14162479>, 2022.

903 Li, D., Overeem, I., Kettner, A. J., Zhou, Y., & Lu, X.: Air temperature regulates erodible
904 landscape, water, and sediment fluxes in the permafrost-dominated catchment on the
905 Tibetan Plateau. Water Resources Research, 57(2),
906 <https://doi.org/10.1029/2020WR028193>, 2021.

907 Liébault, F., Laronne, J. B., Klotz, S., & Bel, C.: Seasonal bedload pulses in a small alpine
908 catchment. Geomorphology, 398, 108055.
909 <https://doi.org/10.1016/j.geomorph.2021.108055>, 2022.

910 Lintunen, K., Kasvi, E., Uvo, C. B., & Alho, P.: Changes in the discharge regime of Finnish
911 rivers. Journal of Hydrology: Regional Studies, 53, 101749,
912 <https://doi.org/10.1016/j.ejrh.2024.101749>, 2024.

913 Lotsari, E., Hackney, C., Salmela, J., Kasvi, E., Kemp, J., Alho, P., and Darby, S. E.:
914 Subarctic river bank dynamics and driving processes during the open-channel flow
915 period. Earth Surf. Process. Landforms, 45: 1198–1216.
916 <https://doi.org/10.1002/esp.4796>, 2020.

917 Lotsari, E., Dietze, M., Kämäri, M., Alho, P., & Kasvi, E.: Macro-Turbulent flow and its
918 impacts on sediment transport potential of a subarctic river during ice-covered and
919 open-channel conditions. Water, 12(7), 1874. <https://doi.org/10.3390/w12071874>,
920 2020.

921 Lotsari, E., Vaaja, M., Flener, C., Kaartinen, H., Kukko, A., Kasvi, E., ... & Alho, P.: Annual
922 bank and point bar morphodynamics of a meandering river determined by high-
923 accuracy multitemporal laser scanning and flow data. Water Resources Research,
924 50(7), 5532-5559. <https://doi.org/10.1002/2013WR014106>, 2014

925 Lotsari, E., de Vet, M., Murphy, B., McLelland, S., and Parsons, D.: Defrosting river banks:
926 morphodynamics and sediment flux, EGU General Assembly 2024, Vienna, Austria,
927 14–19 Apr 2024, EGU24-10175, <https://doi.org/10.5194/egusphere-egu24-10175>,
928 2024.

929 Luoto, M., Heikkinen, R.K. and Carter, T.R.: Loss of palsa mires in Europe and biological
930 consequences. *Environmental conservation*, 31(1), pp. 30–37.
931 Doi:10.1017/s0376892904001018, 2004.

932 Malutta, S. Kobiyama, M. Borges Chaffe, P-L. Bernardi Bonumá, N; Hysteresis analysis to
933 quantify and qualify the sediment dynamics: state of the art. *Water Science*
934 *Technology*; 81 (12): 2471–2487, <https://doi.org/10.2166/wst.2020.279> , 2020.

935 Mao, L.: The effect of hydrographs on bed load transport and bed sediment spatial
936 arrangement, *J. Geophys. Res.* 117, F03024,. doi:10.1029/2012JF002428, 2012.

937 Mao, L.: The effects of flood history on sediment transport in gravel-bed rivers.
938 *Geomorphology*, 322, 196-205. <https://doi.org/10.1016/j.geomorph.2018.08.046>,
939 2018.

940 Matti, B., Dahlke, H., Dieppois, B., Lawler, D., & Lyon, S.: Flood seasonality across
941 Scandinavia—Evidence of a shifting hydrograph? *Hydrological Processes*, 31(24),
942 4354-4370. <http://dx.doi.org/10.1002/hyp.11365>, 2017.

943 Martin, R. L. and D. J. Jerolmack: Origin of hysteresis in bed form response to unsteady
944 flows, *Water Resour. Res.* 49, 1314–1333,. doi:10.1002/wrcr.20093, 2013.

945 Meriö, L. J., Ala-aho, P., Linjama, J., Hjort, J., Kløve, B., & Marttila, H. (2019). Snow to
946 precipitation ratio controls catchment storage and summer flows in boreal headwater
947 catchments. *Water Resources Research*, 55(5), 4096-4109.

948 Micheletti, N., Chandler, J., & Lane, S.: Near instantaneous production of digital terrain
949 models in the field using smartphone and Structure-from-Motion photogrammetry. In
950 EGU General Assembly Conference Abstracts (pp. EGU2013-10501), 2013.

951 Mohammadzadeh Khani H, Kinnard C, Lévesque E.: Historical Trends and Projections of
952 Snow Cover over the High Arctic: A Review. *Water*. 14(4):587.
953 <https://doi.org/10.3390/w14040587>, 2022.

954 Najafi, S., Dragovich, D., Heckmann, T., & Sadeghi, S. H.: Sediment connectivity concepts
955 and approaches. *Catena*, 196, 104880.
956 <https://doi.org/10.1016/j.catena.2020.104880>, 2021.

957 Tananaev, N. I: Hysteresis effects of suspended sediment transport in relation to
958 geomorphic conditions and dominant sediment sources in medium and large rivers
959 of the Russian Arctic. *Hydrology Research* 1 April 2015; 46 (2): 232–243.
960 <https://doi.org/10.2166/nh.2013.199>, 2015.

961 Phillips, C. B., Hill, K. M., Paola, C., Singer, M. B., & Jerolmack, D. J.: Effect of flood
962 hydrograph duration, magnitude, and shape on bed load transport dynamics.
963 *Geophysical Research Letters*, 45, 8264–8271.
964 <https://doi.org/10.1029/2018GL078976>, 2018.

965 Pulliainen, J., Luojus, K., Derksen, C. et al.: Patterns and trends of Northern Hemisphere
966 snow mass from 1980 to 2018. *Nature* 581, 294–298, [https://doi.org/10.1038/s41586-](https://doi.org/10.1038/s41586-020-2258-0)
967 020-2258-0, 2020.

968 Reesink, A. J., & Bridge, J. S.: Evidence of bedform superimposition and flow unsteadiness
969 in unit-bar deposits, South Saskatchewan River, Canada. *Journal of Sedimentary*
970 *Research*, 81(11), 814-840. <https://doi.org/10.2110/jsr.2011.69> , 2011.

971 Salmela, J., Kasvi, E., Vaaja, M. T., Kaartinen, H., Kukko, A., Jaakkola, A., & Alho, P.:
972 Morphological changes and riffle-pool dynamics related to flow in a meandering river
973 channel based on a 5-year monitoring period using close-range remote sensing.
974 *Geomorphology*, 352, 106982. <https://doi.org/10.1016/j.geomorph.2019.106982>,
975 2020.

976 Sen, P. K.: Estimates of the regression coefficient based on Kendall's tau. *Journal of the*
977 *American statistical association*, 63(324), 1379-1389.
978 <https://doi.org/10.1080/01621459.1968.10480934>, 1968.

979 Syvitski, J. P.: Sediment discharge variability in Arctic rivers: implications for a warmer
980 future. *Polar Research*, 21(2), 323-330. <https://doi.org/10.3402/polar.v21i2.6494>,
981 2002.

982 Shrestha, R.R., Bennett, K.E., Peters, D.L., Yang, D.: Hydrologic Extremes in Arctic Rivers
983 and Regions: Historical Variability and Future Perspectives. In: Yang, D., Kane, D.L.
984 (eds) *Arctic Hydrology, Permafrost and Ecosystems*. Springer, Cham. 2021.

985 van Rooijen, E., & Lotsari, E., 2024 The spatiotemporal distribution of river bank erosion
986 events and their drivers in seasonally frozen regions, *Geomorphology*, Volume 454.
987 <https://doi.org/10.1016/j.geomorph.2024.109140>, 2024.

988

989 Vatne, G., Takøy Naas, Ø., Skårholen, T., Beylich, A. A., & Berthling, I.: Bed load transport
990 in a steep snowmelt-dominated mountain stream as inferred from impact sensors.
991 *Norsk Geografisk Tidsskrift-Norwegian Journal of Geography*, 62(2), 66-74.
992 <https://doi.org/10.1080/00291950802094817>, 2008.

993 Veijalainen, N., Lotsari, E., Alho, P., Vehviläinen, B., & Käyhkö, J.: National scale
994 assessment of climate change impacts on flooding in Finland. *Journal of hydrology*,
995 391(3-4), 333-350. <https://doi.org/10.1016/j.jhydrol.2010.07.035>, 2010.

996 Viglione, A., Chirico, G. B., Komma, J., Woods, R., Borga, M., & Blöschl, G.: Quantifying
997 space-time dynamics of flood-event types. *Journal of Hydrology*, 394(1-2), 213-229.
998 <https://doi.org/10.1016/j.jhydrol.2010.05.041>, 2010.

999 Vormoor, K., Lawrence, D., Schlichting, L., Wilson, D., & Wong, W. K.: Evidence for changes
1000 in the magnitude and frequency of observed rainfall vs. snowmelt driven floods in
1001 Norway. *Journal of Hydrology*, 538, 33-48.
1002 <https://doi.org/10.1016/j.jhydrol.2016.03.066>, 2016.

1003 Wenng, H., Barneveld, R., Bechmann, M., Marttila, H., Krogstad, T., & Skarbøvik, E.:
1004 Sediment transport dynamics in small agricultural catchments in a cold climate: a
1005 case study from Norway. *Agriculture, Ecosystems & Environment*, 317, 107484.
1006 <https://doi.org/10.1016/j.agee.2021.107484>, 2021.

1007 Williams, G. P.: Sediment concentration versus water discharge during single hydrologic
1008 events in rivers. *Journal of Hydrology*, 111(1-4), 89-106.
1009 [https://doi.org/10.1016/0022-1694\(89\)90254-0](https://doi.org/10.1016/0022-1694(89)90254-0), 1989.

1010 Wohl, E.: Connectivity in rivers. *Progress in Physical Geography*, 41(3), 345-362.
1011 <https://doi.org/10.1177/0309133317714972>, 2017.

1012 Zhang, T., Li, D., Kettner, A. J., Zhou, Y., & Lu, X.: Constraining dynamic sediment-discharge
1013 relationships in cold environments: The sediment-availability-transport (SAT) model.
1014 *Water Resources Research*, 57(10), <https://doi.org/10.1029/2021WR030690>, 2021.

1015 Zhang, T., Li, D., East, A.E. et al. Warming-driven erosion and sediment transport in cold
1016 regions. *Nat Rev Earth Environ* 3, 832–851, <https://doi.org/10.1038/s43017-022-00362-0>, 2022.

1017

1018 Zhang, T., Li, D., East, A. E., Kettner, A. J., Best, J., Ni, J., & Lu, X.: Shifted sediment-
1019 transport regimes by climate change and amplified hydrological variability in
1020 cryosphere-fed rivers. *Science Advances*, 9(45). DOI: 10.1126/sciadv.adi5019, 2023.

1021

